Magnesium Technology 2012
Edited by: Suveen N. Mathaudhu, Wim H. Sillekens, Neale R. Neelameggham, and Norbert Hort
TMS (The Minerals, Metals & Materials Society), 2012

EFFECT OF SOME MICROSTRUCTURAL PARAMETERS ON THE CORROSION RESISTANCE OF MAGNESIUM ALLOYS

Yaning Hu[1], Joseph R. Kish[1], Joseph R. McDermid[1], Wenyue Zheng[2]
[1]Centre for Automotive Materials and Corrosion, McMaster University, 1280 Main St. W., Hamilton, ON, L8S 4L7 Canada
[2]CANMET-MTL, 183 Longwood Rd. S., Hamilton, ON, L8P 0A5 Canada

Keywords: Magnesium Alloys, Microstructure, Corrosion

Abstract

The influence of the β-$Mg_{17}Al_{12}$ phase and, to a lesser degree, the solute content in the α-Mg matrix on the corrosion resistance of Mg alloys was investigated by cyclic potentiodynamic polarization and potentiostatic polarization tests using AZ31B, AM30 and AM60B in contact with a mildly aggressive near-neutral saline solution. Results showed that all three Mg alloys corrode in a partially protective state under open circuit conditions in the test solution. It was also determined that the surface film formed on each exhibits a similar apparent breakdown potential. This indicates that microstructure parameters such as the presence of the β-phase and the solute content of the α-Mg matrix do not strongly influence the factors controlling the breakdown of the surface films formed. It was further determined that the moderately improved protectiveness of the surface film, rather than the distribution of the β-$Mg_{17}Al_{12}$ phase, is responsible for the improved (short-term) corrosion resistance exhibited by AM60B at potentials below the breakdown potential.

Introduction

Reducing the overall mass of automobiles by increased utilization of Mg alloys is one of the means by which improved fuel efficiency and reduced harmful emissions can be attained. The 2020 strategic goal of the North American-based automotive manufacturers is to substitute 340 lbs. of Mg components for 630 lbs. of current carbon steel and Al alloy parts (290 lbs. weight saved), bringing the total average vehicle Mg content to 350 lbs. [1]. The multi-national MFERD (magnesium front end research and development) project is one major effort towards reaching this goal. The objectives of the project are to develop: (i) key enabling technologies in Mg extrusion, sheet, high-integrity body casting, joining and assembly, and (ii) a knowledge base for increased Mg automotive body applications in corrosion protection, crashworthiness, fatigue, durability and NHV (noise, harshness and vibration) performance [2]. The Mg alloys of choice for the assembly include AZ31 sheet, AM30 extrusions and AM60B die castings.

The corrosion resistance of Mg alloys is a major technological issue preventing widespread application. It is strongly influenced by the alloy composition, microstructure and the formation of a partially-protective surface film. Controlling factors for Mg alloys containing Al, Zn and Mn include the solid solution α-matrix, secondary β-phase ($Mg_{17}Al_{12}$) formed along grain boundaries and intermetallic $Al_xMn_yFe_z$ particles [3-5]. Alloyed Al modifies the composition of the surface film formed on both the α-matrix and β-phase [6]. Recent studies indicate that an increased Al content improves the corrosion resistance in moist air [7], salt spray [8], and aqueous Cl^--containing solutions [9]. The β-phase, which is an effective cathode with a corrosion potential more positive than that of the α-matrix, may accelerate the anodic dissolution of the α-phase by establishing a microgalvanic cell [10-12]. Both the grain size of the α-matrix and the distribution of the β-phase are important factors, as the β-phase can act either as an effective cathode (coarse-grain α-matrix and discontinuous β-phase) or as a corrosion barrier (fine-grain α-matrix and continuous β-phase) [10-12]. The $Al_xMn_yFe_z$ particles, also with a corrosion potential more positive than that of the α-matrix, can act as effective cathodes and accelerate the anodic dissolution of the α-phase, albeit in a more localized manner than that produced by the β-phase [1,11,13].

Standard cyclic salt spray testing is a common method to evaluate the corrosion resistance of Mg alloys exposed to more-realistic, on-vehicle conditions. Comparative corrosion performance data for the three MFERD Mg alloys, using such test methods, is now being reported in the open literature [14]. While these tests are instructive from a relative corrosion performance perspective, they provide little insight into the important, yet subtle differences in electrochemical behavior. Such information is required for a more complete mechanistic understanding of the observed performance. To address this need, in support of the MFERD effort, cyclic potentiodynamic anodic polarization and potentiostatic polarization tests were conducted using the MFERD Mg alloys (AM30, AZ31B and AM60B) in contact with the mildly aggressive near-neutral saline solution utilized in the GMW14872 (Cyclic Corrosion Laboratory Test) Standard.

Experimental Details

The composition of the three Mg alloys tested is shown in Table I. Significant differences include the Zn content between AZ31B and AM30 and the Al content between AM30 and AM60B. The as-received AZ31B sheet was given a recrystallization heat treatment at 350°C for 6 h. No heat treatments of any kind were performed on the as-received extruded AM30 bar or the die-cast AM60B sheet.

Table I. Composition (wt.%) of Mg Alloys

Alloy	Al	Zn	Mn	Fe	Si
AZ31B	3.1	0.96	0.43	0.002	0.02
AM30	2.7	< 0.01	0.42	0.014	< 0.01
AM60B	5.6	0.10	0.34	0.007	0.02

Figure 1 shows the cross-sectional microstructure normal to the longitudinal direction (rolling direction of AZ31 sheet and extrusion direction of AM30 bar) of the three Mg alloys. The microstructure of both 3 wt.% Al-containing alloys (AZ31B and AM30) revealed an equiaxed-grain α-matrix that contained randomly distributed Al-Mn intermetallic particles (confirmed by SEM-EDS). In contrast, the microstructure of the 6 wt.% Al-containing AM60B revealed a discontinuous network of β-phase precipitates along the α-matrix grain boundaries. Both the

extruded AM30 and die-cast AM60B exhibited a distinct surface/ skin layer; a coarse-grain skin on a fine-grained interior for the extruded AM30 and a fine-grain skin on a coarse-grained interior for the die-cast AM60B. The spherical pit-like features are an artifact of the mechanical polishing procedure employed.

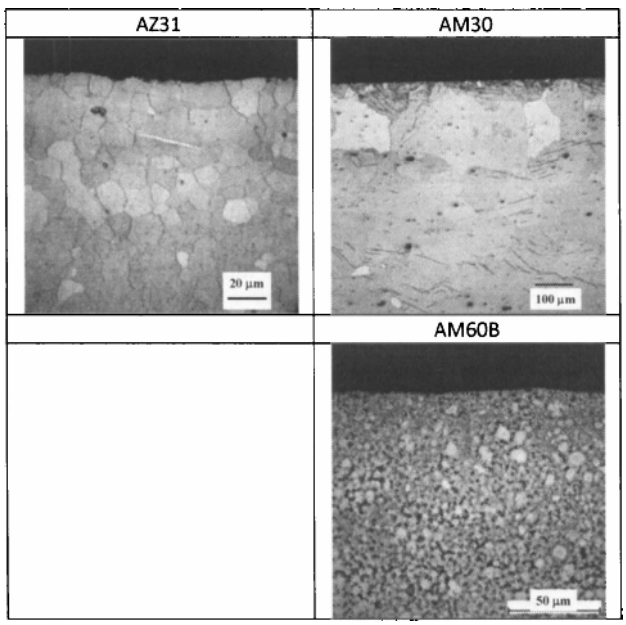

Figure 1. Cross-sectional microstructures normal to the longitudinal direction (rolling direction of AZ31B sheet and extrusion direction of AM30 bar) of the three Mg alloys studied. Note the varying magnifications between the micrographs.

Electrochemical measurements were made in the GMW14872 test solution (9 wt.% NaCl, 0.1 wt.% $CaCl_2$ and 0.25 wt.% $NaHCO_3$) with pH 7.9 at room temperature. No attempt was made to aerate or deaerate the solution. Measurements were conducted using a standard three electrode test cell with a volume of 1000 mL. All working electrodes were prepared by cold mounting a small square sample (1 cm^2) in epoxy resin. Electrical contact was obtained by adhesive joining a Cu wire to the back side of the working electrode prior to cold mounting. This Cu lead was inserted into a plastic tube, which was then sealed to the back of the epoxy resin mount using epoxy resin. The majority of working electrodes prepared in this way were ground to a 1200 grit surface finish using SiC paper and absolute ethanol (100%) as a lubricant, then dried in cool air prior to immersion. This mechanically polishing (MP) procedure successfully removed the skin layer in the AM30 and AM60B electrodes. Consequently, additional electrodes were prepared from AM30 and AM60 in the as-received condition (AR), without mechanical polishing, to evaluate the polarization behavior of the skin layer. All electrochemical tests were performed using either an EG&G Model 273 potentiostat or a GAMRY Reference 600 potentiostat with a graphite rod counter electrode. All electrode potentials were measured against a standard calomel (SCE) reference electrode.

All polarization measurements were initiated after the Mg alloy electrode was aged at the corrosion potential for 1h. The cyclic potentiodynamic anodic polarization measurement was initiated at -0.25 V versus the corrosion potential and was reversed at +0.50 V versus the corrosion potential. The scan rate was 1 mV/s. Anodic potentiostatic polarization measurements were made at an applied potential just below the apparent breakdown potential for a hold time of 2 h and at an applied potential just above the apparent breakdown potential for a hold time of 0.5 h. Cathodic potentiostatic polarization measurements were made at an applied potential of -1.8 V_{SCE} for a hold time of 2 h.

Results

Potentiodynamic Measurements

Figure 2 shows the cyclic potentiodynamic anodic polarization curves measured on the MP surface of the three Mg alloys. All three curves exhibit a similar general behavior, namely an apparent anodic breakdown potential, above which the anodic current density increases markedly, and an apparent repassivation potential following a hysteresis loop upon reversing the applied potential. The corrosion potential exhibited by AM60B was significantly more positive than that exhibited by either AM30 or AZ31B. In contrast, both the breakdown potential and the repassivation potential exhibited by the three Mg alloys were similar. The breakdown potential for each of the three Mg alloys was more positive than their respective corrosion potentials, but the repassivation potential of AM60B was more negative than its corrosion potential.

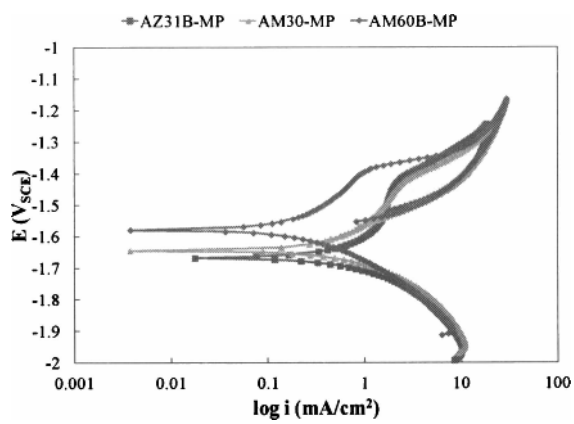

Figure 2. Cyclic potentiodynamic anodic polarization curve for MP surface of AZ31B, AM30 and AM60B after aging for 1 h at the corrosion potential in the GMW14872 test solution at room temperature.

The cyclic potentiodynamic anodic polarization curves measured on the skin and on the interior (polished) surface of extruded AM30 and die cast AM60B are shown in Figure 3. The coarse-grained skin layer of the extruded AM30 exhibited a similar anodic polarization response to that exhibited by the fine-grained interior. In contrast, a marked difference in the response between the fine-grained skin layer and the coarse-grained interior was observed for the die-cast AM60B. The main cause of the marked difference was the more noble corrosion potential exhibited by the fine-grained skin layer. Despite this difference in corrosion potential, both the fine-grained skin layer and the coarse-grained

interior of AM60B exhibited a similar breakdown potential and repassivation potential.

Table II lists selected electrochemical kinetic parameters extracted from the curves presented in Figure 2 & 3. The potentials listed support the comparative observations made above regarding the corrosion (E_{corr}), breakdown (E_b) and repassivation (E_r) potentials. The cathodic Tafel slope (β_c) corresponds to the slope of the linear portion of the cathodic polarization curve, which was assumed to initiate at an applied potential of 50 mV versus the corrosion potential. Both the corrosion current density (i_{corr}) and the exchange current density of the hydrogen evolution cathodic reaction ($i_{o,c}$) were computed by extrapolating the linear (Tafel) portion of the cathodic polarization curve back to the respective corrosion potential and the equilibrium half cell potential of the hydrogen evolution reaction (-0.694 V_{SCE} at pH 7.9). The corrosion current density (rate) exhibited by AM60B was an order of magnitude lower than both AZ31B and AM30, which were similar, The corrosion current density of the skin layer and the interior was of the same order of magnitude for both AM30 and AM60B. Moreover, the exchange current density for the cathodic reaction (hydrogen evolution) estimated for all samples was also within one order of magnitude, with the exception of the AM60B-AR sample, which was an order of magnitude lower.

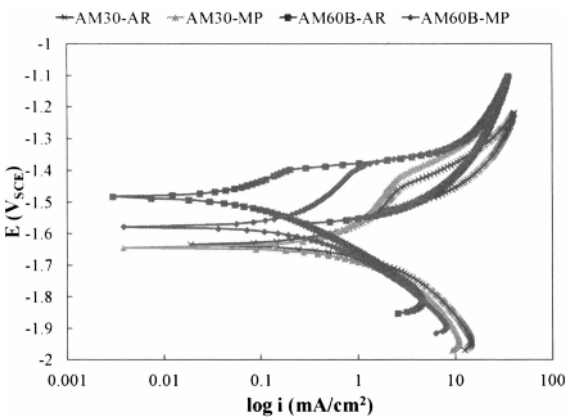

Figure 3. Cyclic potentiodynamic anodic polarization curve for the MP surface and the AR surface of AM30 and AM60B after aging for 1 h at the corrosion potential in the GMW14872 test solution at room temperature.

Table II. Selected Electrochemical Kinetic Parameters

Alloy	E_{corr} V_{SCE}	E_b V_{SCE}	E_r V_{SCE}	β_c (V/dec.)	i_{corr} (A/cm²)	$i_{o,c}$ (A/cm²)
AZ31B-MP	-1.66	-1.43	-1.52	0.215	1.1×10^{-3}	2.5×10^{-8}
AM30-AR	-1.63	-1.46	-1.52	0.202	1.1×10^{-3}	2.3×10^{-8}
AM30-MP	-1.66	-1.42	-1.54	0.213	1.0×10^{-3}	1.2×10^{-8}
AM60B-AR	-1.50	-1.41	-1.57	0.180	1.6×10^{-4}	5.8×10^{-9}
AM60B-MP	-1.56	-1.40	-1.58	0.218	3.7×10^{-4}	4.1×10^{-8}

Potentiostatic Measurements

Figure 4 shows the anodic current density transient recorded on the MP surface in response to the anodic potentiostatic polarization at an applied potential just above and just below the breakdown potential for the three Mg alloys. Also included is the anodic current density transient recorded on the AR surface of AM60B at an applied potential just above the breakdown potential. A measurement on the AR surface of AM60B at an applied potential just below the breakdown potential was not attempted since the corrosion potential was 90 mV more negative than the breakdown potential. The AR surface of AM30 was not tested since it exhibited essentially the identical cyclic polarization behavior as observed for the MP surface. All anodic current density transient exhibited a similar behavior, namely an initial rapid increase followed by a much slower decay from the maximum value obtained. The anodic current density was at least one order of magnitude lower at an applied potential just below the breakdown potential than that exhibited at an applied potential just above the breakdown potential for all three Mg alloys. The anodic current density transient measured on the MP surface was lowest for the die-cast AM60B at both applied potentials. The difference in magnitude of the anodic current density exhibited by the AM60B-MP compared to that exhibited by the other two Mg alloys was greater (an order of magnitude lower) for the applied potential below the apparent breakdown potential.

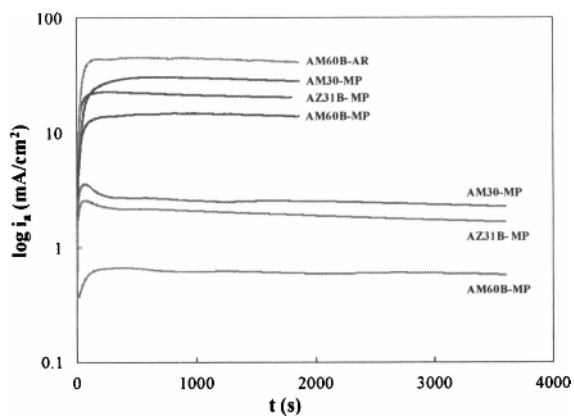

Figure 4. Anodic current transient for the MP surface of the three Mg alloys and the AR surface of AM60B in the GMW14872 test solution at room temperature for an applied potential just above (upper transients) and below (lower transients) the breakdown potential in the GMW14872 test solution at room temperature.

Photographs of the MP surface of AM60B after the potentiostatic anodic polarization experiment are shown in Figure 5. There was little evidence of corrosion observed on the surface exposed at an applied potential just below the breakdown potential. The surface was dull grey and macroscopically smooth in appearance. In contrast, there was significant corrosion observed on the surface exposed at an applied potential just above the breakdown potential. The corrosion mode best resembled extensive pitting corrosion. A similar set of observations was extracted for the MP surface of the two AZ31B and the two AM30 samples exposed to similar conditions.

Light optical microscope images of the MP surface cross-sections for the three Mg alloys after potentiostatic anodic polarization experiments are shown in Figure 6. Superficial corrosion attack was observed on each of the three Mg alloy surfaces held at an applied potential just below the breakdown potential. In contrast, significant corrosion attack was observed on each of three Mg alloy surfaces held at an applied potential just above the breakdown potential. This significant corrosion attack was pit-like in appearance and tended to spread laterally across the surface rather than propagate deep into the Mg alloy sample.

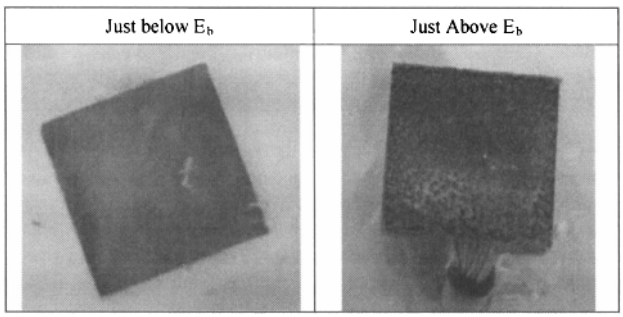

Figure 5. Photograph of the MP surface for AM60B (~1cm^2) after potentiostatic anodic polarization at an applied potential just above and just below the breakdown potential (E_b) in the GMW14872 test solution at room temperature.

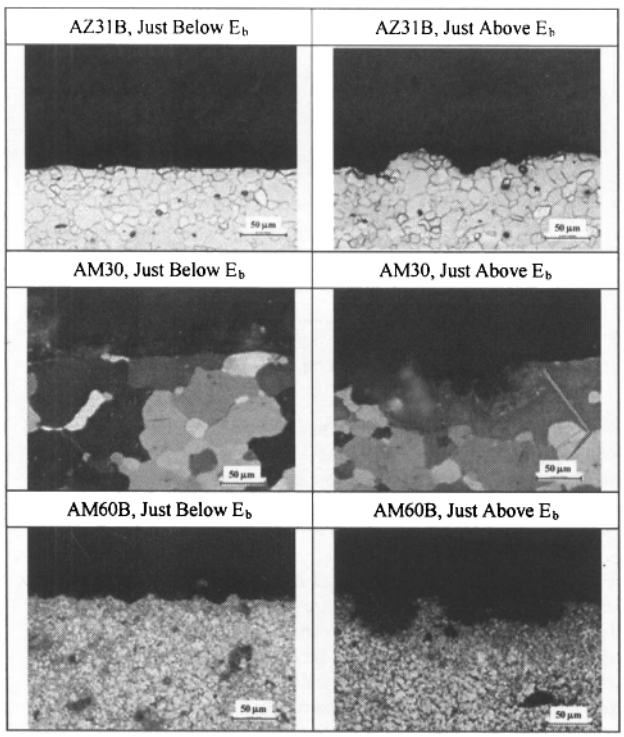

Figure 6. Light optical microscope images of the MP surface, in cross-section, for the three Mg alloys after potentiostatic anodic polarization at an applied potential above and below the breakdown potential (E_b) in the GMW14872 test solution at room temperature.

Figure 7 shows the cathodic current density transient recorded on the MP surface of the three Mg alloys in response to the cathodic potentiostatic polarization at an applied potential of -1.8 V_{SCE}. Also included is the cathodic current density transient recorded on the AR surface of AM60B. All cathodic current density transients exhibited a similar behavior, namely an initial increase followed by the establishment of a reasonably steady state value. The initial increase was relatively rapid except for AZ31B. Moreover, the steady state current density was established at the maximum value except for the AR surface of AM60B, on which the steady state current density was attained after a decay from the maximum value. Regardless on the initial transient behavior, the steady state current density attained after 1 h exposure was within the same order of magnitude for each case.

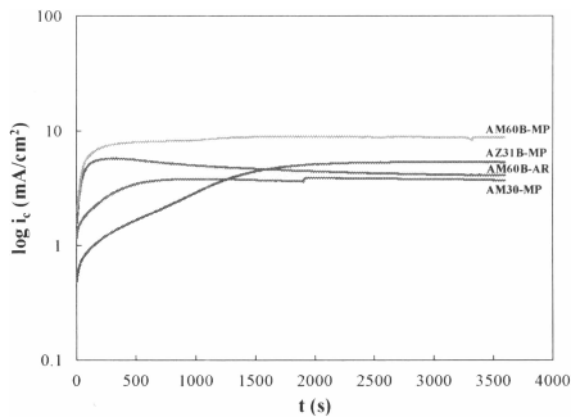

Figure 7. Cathodic current transient for the MP surface of the three Mg alloys and the AR surface of AM60B at an applied potential of -1.8 V_{SCE} in the GMW14872 test solution at room temperature.

Discussion

Based on the anodic polarization behavior (Figure 2 & 3), all three Mg alloys, regardless of the surface condition exposed, corrode at a potential that is below the breakdown potential after aging for 1 h in the GMW14872 test solution at room temperature. Both the steady state applied anodic current density transients (Figure 4) and the cross-section images (Figure 6) indicate that all three Mg alloys corrode in a partially protected state at these potentials (below the breakdown) for all three Mg alloys. Moreover, the relative differences observed in the anodic current density transients, at an applied potential below the breakdown potential (Figure 4), and in the cathodic current density transients (Figure 7) indicate that the improved relative corrosion resistance of AM60B was controlled primarily by the anodic kinetics. The significance of these findings is discussed in some detail below.

The presence of a breakdown potential in the anodic polarization behavior of AZxx Mg alloys in mildly aggressive aqueous salt (Cl^-, SO_4^{2-} and HCO_3^-) solutions has been well documented [14-16]. However, a consensus on a micro-mechanisms involved has not yet been attained. The majority of the focus has been placed on delineating the role played by the the microgalvanic interaction between the α matrix and an adjacent effective cathodic phase, such as AlMn intermetallic particles and/or the β phase [4,9,10]. The role by the aggressive anion (Cl^-) in the film breakdown

process has received little attention in this context. However, the incorporation of the aggressive anion (Cl^-) into the surface film at weak points and the subsequent formation of soluble magnesium hydroxychloride complexes has been tenuously proposed to explain the observed behaviour [17,18].

In this study the breakdown potential is essentially the same for all three Mg alloys, regardless of the surface condition exposed. This suggests that a common factor controls the breakdown process. If true, then any factor associated with the β–phase can be ruled out, since it was not present in either AZ31B or AM30. Given that AlMn intermetallic particles are present in all three Mg alloys, any associated factors cannot be directly ruled out. However, at potentials below the breakdown potential, the cathodic (hydrogen evolution) reaction is believed to occur on the relatively thick surface film rather than on the Mg alloy substrate [6,19]. If true, then it seems unlikely that the AlMn intermetallic particles present at the interface between the relatively thick surface film and the Mg alloy substrate could act as effective cathodes causing the surface film to locally break down.

It follows that the controlling factor may indeed be the migration of the aggressive anion (Cl^-) into the surface film at weak points. A common breakdown potential would require that the bulk composition of the surface film formed on the three Mg alloys to be largely similar in composition. A recently reported XPS study on the composition of the surface film formed after short exposure to 0.1 N NaCl solutions show this to be the case for AZxx alloys [20]. The surface film is typically comprised of a mixed $Mg(OH)_2$-$MgCO_3$ outer layer on a mixed $Mg(OH)_2$-MgO inner layer. A similar, albeit minor, Al content independent of the concentration in the bulk alloy was observed in the surface film after sputtering.

A comparison of the corrosion rate data (Table II) suggests that there is a meaningful difference between the three Mg alloys, with AM60B exhibiting the highest relative corrosion resistance. It is recognized that a poor manual fit of the cathodic Tafel slope, as done in this study, can change the extrapolated corrosion current density (rate) by a factor between 5 and 10 [21]. Such a maximum error (factor of 10) would discount the observation that there is a meaningful difference in the corrosion rate. However, the order of magnitude improved relative corrosion resistance exhibited by AM60B based on the cathodic Tafel extrapolated corrosion current density (Table II) is consistent with that based on the steady state anodic current density attained at an applied potential below the breakdown potential (Figure 4). This agreement gives a level of confidence that this difference is significant. Thus, the relative ranking of corrosion resistance, at a potential below the breakdown potential, in the GMW14872 solution is given by:

$$AM60B > AM30 \approx AZ31B$$

Of the two half-cell processes involved in the corrosion cell, the anodic process was observed to be chiefly responsible for the order of magnitude lower relative corrosion current density (rate) exhibited by AM60B. The cathodic (hydrogen evolution) process is discounted based on the observation that there was no significant difference in either the order of magnitude of the extrapolated exchange current density or the steady state cathodic current density attained an applied potential of -1.8 V_{SCE} exhibited by the three Mg alloys. However, similar cathodic kinetics do indicate that neither the solute (Zn) content of the α-matrix nor the presence of the β-phase has a significant influence at a corrosion potential less than the breakdown potential.

Regarding the anodic process, the root cause of the improved corrosion resistance of AM60B is unclear. However, it is not likely the result of a continuous β-phase barrier layer present at the alloy surface. If true, then differences would be expected in both the breakdown potential and the cathode kinetics, compared to that exhibited by either AZ31B or AM30, based on the reported electrochemical polarization behavior of the β-phase in an aqueous Cl^--containing solution [9]. Based on the essentially identical anodic kinetics exhibited by Zn-containing AZ31B and non Zn-containing AM30, the root cause is also likely not the result of the solute Zn content in the a-matrix

It is noted that this observed improved corrosion resistance (AM60B relative to both AZ31B and AM30) is consistent with a reported study comparing the corrosion resistance between of AZ31 and AZ91 in mildly aggressive aqueous Cl^--containing solutions, in which the corrosion potential was below the breakdown potential [20]. In that study, the improved corrosion resistance was tentatively attributed to MgO as the dominant surface film component. Clearly a detailed compositional analysis of the surface films formed during the exposure at a corrosion potential less than the breakdown potential is required to better understand the root cause of the improved corrosion resistance exhibited by the β-phase containing Mg alloys.

Conclusions

1. Electrochemical polarization measurements after short exposures were instructive in providing more insight into the important, yet subtle differences in electrochemical behavior exhibited by AZxx and AMxx Mg alloys when exposed at potentials below the breakdown potential.

2. The overall relative ranking of corrosion resistance, at a potential below the breakdown potential, in the GMW14872 solution is given by: AM60B > AM30 ≈ AZ31B. This relative ranking is controlled more so by the anodic kinetics rather than the cathode kinetics. An improved protectiveness of the surface film, rather than the distribution of the β-$Mg_{17}Al_{12}$ phase, appears to be responsible for the improved corrosion resistance of AM60B (regardless of surface condition).

3. All three Mg alloys exhibited no significant differences in breakdown potential. This indicates that microstructure aspects such as the solute content in the α-Mg matrix and the presence of the β-phase do not strongly influence the factors controlling the breakdown of the surface films formed.

Acknowledgments

This work was financially supported by Natural Resources Canada (CANMET-MTL) and the Natural Sciences and Engineering Research Council of Canada (NSERC). The authors also wish to thank D. Culley of the Department of Materials Science and Engineering at McMaster University for his technical support with metallographic sample preparation. Thanks also to GM for providing samples of the MFERD Mg alloy.

References

1. G. Cole, "Summary of Magnesium Vision 2020: A North American Automotive Strategic Vision for Magnesium," *Magnesium Technology 2007*, ed. R.S. Beals et al., (Warrendale, PA: TMS, 2007), 35-40.
2. E.A. Nyberg et al., "Magnesium for Future Autos," *Adv. Mater. Processes*, 166 (10) (2008), 35-37.
3. G.L Makar, J. Kruger, "Corrosion of Magnesium," *Int. Mater. Rev.*, 38 (1993), 138-153.
4. G. Song and A. Atrens, "Understanding Magnesium Corrosion: A Framework for Improved Alloy Performance," *Adv. Eng. Mater.*, 5 (2003), 837-858.
5. E. Ghali et al., "General and Localized Corrosion of Magnesium Alloys: A Critical Review," *J. Mater. Eng. Perform.*, 13 (2004), 7-23.
6. G. L. Song et al., "Corrosion Behaviour of AZ21, AZ501 and AZ91 in Sodium Chloride," *Corros. Sci.*, 40 (1998), 1769-1791.
7. M. Jonsson and D. Persson, "The Influence of Microstructure on the Atmospheric Corrosion Behaviour of Magnesium Alloys AZ91D and AM50," *Corros. Sci.*, 52 (2010), 1077-1085.
8. G. Ballerini et al., "About Some Corrosion Mechanisms of AZ91D Magnesium Alloy," *Corros. Sci.*, 47 (2005), 2173-2184.
9. A. Pardo et al., "Corrosion Behaviour of Magnesium/ Aluminum Alloys in 3.5 wt.% NaCl," *Corros. Sci.*, 50 (2008), 823-834.
10. O. Lunder et al., "The Role of $Mg_{17}Al_{12}$ Phase in the Corrosion of Mg Alloy AZ91," *Corrosion*, 45 (1989), 741-748.
11. G. L. Song and A. Atrens, "Corrosion Mechanisms of Magnesium Alloys," *Adv. Eng. Mater.*, 1 (1999), 11-33.
12. G. L. Song, "Recent Progress in the Corrosion and Protection of Magnesium Alloys," *Adv. Eng. Mater.*, 7 (2005), 563-586.
13. O. Lunder et al., "Effect of Mn Additions on the Corrosion Behaviour of Mould-Cast Magnesium ASTM AZ91," *Corrosion*, 43 (1987), 291-295.
14. M-C. Zhao et al., "An Exploratory Study of the Corrosion of Mg Alloys during Interrupted Salt Spray Testing," *Corros. Sci.*, 51 (2009), 1277-1292.
15. L. Wang et al., "Influence of Chloride, Sulfate and Bi-carbonate Anions on the Corrosion Behavior of AZ31 Magnesium Alloy," *J. Alloy Compd.*, 496 (2010) 500–507.
16. L. Wang et al., "Corrosion Behavior of Mg, AZ31, and AZ91 Alloys in Dilute NaCl Solutions," *J. Solid State Electrochem.*, 14 (2010), 1897-1907.
17. R. Tunold et al., "The Corrosion of Magnesium in Aqueous Solution Containing Chloride Ions," *Corros. Sci.* 17 (1977), 353-365.
18. G. Williams and H.N. McMurray, "Localized Corrosion of Magnesium in Chloride-Containing Electrolyte Studied by a Scanning Vibrating Electrode Technique," *J. Electrochem. Soc.*, 155 (7) (2008), C340-C349.
19. G. Song et al., "The Electrochemical Corrosion of Pure Magnesium in 1 N NaCl," *Corros. Sci.*, 39 (1997), 855-875.
20. L. Wang et al., "XPS Study of the Surface Chemistry on AZ31 and AZ91 Magnesium Alloys in Dilute NaCl Solution," *Appl. Surf. Sci.*, 256 (2010) 5807-5812.
21. R.G. Kelly, "Electrochemical Thermodynamics and Kinetics of Relevance to Corrosion," *Electrochemical Techniques in Corrosion Science and Engineering*, ed. R.G. Kelly et al., (New York, NY: Marcel Dekker, Inc. 2003), 45.